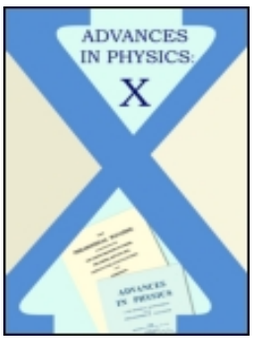

Advances in Physics: X

ISSN: (Print) 2374-6149 (Online) Journal homepage: http://www.tandfonline.com/loi/tapx20

Electronic shell structures in bare and protected metal nanoclusters

Hannu Häkkinen

To cite this article: Hannu Häkkinen (2016) Electronic shell structures in bare and protected metal nanoclusters, Advances in Physics: X, 1:3, 467-491, DOI: 10.1080/23746149.2016.1219234

To link to this article: http://dx.doi.org/10.1080/23746149.2016.1219234

Published online: 16 Aug 2016.

ADVANCES IN PHYSICS: X, 2016
VOL. 1, NO. 3, 467–491
http://dx.doi.org/10.1080/23746149.2016.1219234

Taylor & Francis
Taylor & Francis Group

REVIEW ARTICLE

OPEN ACCESS

Electronic shell structures in bare and protected metal nanoclusters

Hannu Häkkinen

Departments of Physics and Chemistry, Nanoscience Center, University of Jyväskylä, Jyväskylä, Finland

ABSTRACT

This short review discusses the concept of the electronic shell structure in the context of metal nanoclusters. Electronic shell structure is a natural consequence of quantization of fermionic states in a quantum confinement, where the symmetry of the confining potential creates energetically close-lying sets of states that reflect the symmetry of the potential. It was introduced in cluster physics in early 1980s and initially influenced greatly by the related model of nuclear shell structure from 1950's. Three application areas are discussed consisting of free gas phase clusters, clusters supported by insulating oxides or oxide thin films, and clusters that are synthesized by wet chemistry and stabilized by an organic ligand layer. In all these systems, the concept of electronic shell structure has turned out to be useful to organize a vast amount of observations on abundance, stability, chemical reactivity and optical properties. Although this review focuses on theoretical concepts and computational results, relevant experiments are discussed as well.

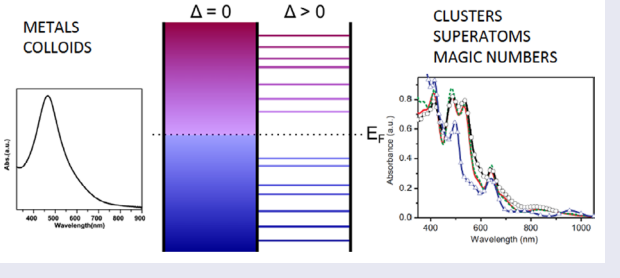

ARTICLE HISTORY
Received 9 May 2016
Accepted 26 July 2016

KEYWORDS
Nanocluster; noble metal; simple metal; magic numbers; superatom; ligand-stabilized nanocluster

PACS
36.40.Cg Electronic and magnetic properties of clusters; 36.40.Jn Reactivity of clusters; 36.40.Vz Optical properties of clusters; 61.46.Bc Structure of clusters

1. Introduction: quantum size effects and the fundamental energy gap

Every undergraduate textbook of solid state physics contains a discussion of a 'perfect theorist's metal': the three-dimensional electron gas of N electrons

CONTACT Hannu Häkkinen hannu.j.hakkinen@jyu.fi

confined in volume V, where the electrons interact only by virtue of being fermions, i.e. obeying the Pauli exclusion principle. In such system, the dispersion relation for the electron states is parabolic ($E \propto \mathbf{k}^2$) where $\mathbf{k}$ is the wave vector in reciprocal space. The available $N/2$ quantum states are filled by N electrons up to the Fermi energy E_F. The density of electron states $D(E)$ follows a square-root behavior as a function of the electron energy,

$$D(E) = \frac{3}{2} N \frac{\sqrt{E}}{E_F^{3/2}} \tag{1}$$

which leads to a simple estimate of D at the Fermi energy

$$D(E_F) = \frac{3N}{2E_F} \tag{2}$$

In macroscopic metal, the density of states has a finite value at E_F. As discussed long ago by Fröhlich [1] and Kubo [2], confining electrons in a nanometer-scale volume discretizes the allowed levels and thus can create an energy gap Δ also at the Fermi level (Figure 1). The existence of this fundamental gap (or 'band gap') changes profoundly the physical properties of the system since the external perturbations thus need to have a minimum energy to excite electrons over the band gap. Conventionally, the magnitude of the gap has been taken as a measure to classify systems into 'metallic' (with Δ approaching zero), 'semiconducting' or 'insulating'. For practical matters, systems have been considered 'metallic' when Δ is of the order of the thermal energy at room temperature ($k_B T_R \approx 25$ meV).

This criterion leads to interesting predictions regarding the critical size (diameter d_{cr}) where Δ exceeds $k_B T_R$ as the size of the system is decreased. From Equation (2), the mean spacing of electron levels at E_F is simply

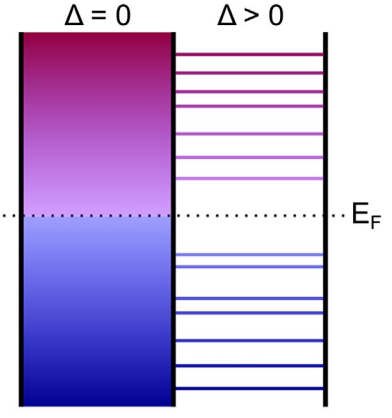

Figure 1. A schematic representation of the electron states in bulk metal (left) and in a nanoparticle (right). The energy gap Δ is zero in the bulk metal while the gap is nonzero in the nanoparticle. E_F denotes the Fermi energy.

Table 1. Critical diameters and number of electrons for metal clusters where the 'Kubo gap' equals the thermal energy. Values for the free electron density and Fermi energy are taken from Ref. [3].

	Z	n_{free} (1/nm^3)	E_F (eV)	N_{cr}	d_{cr} (nm)
Li	1	47.0	4.72	126	1.7
Na	1	26.5	3.23	86	1.8
K	1	14.0	2.12	57	2.0
Cu	1	84.5	7.00	187	1.6
Ag	1	58.5	5.48	146	1.7
Au	1	59.0	5.51	147	1.7
Mg	2	86.0	7.13	190	1.6
Ca	2	46.0	4.68	125	1.7
Zn	2	131.0	9.39	250	1.5
Al	3	180.6	11.63	310	1.5
Ga	3	153.0	10.35	276	1.5

$$\Delta = \frac{1}{D(E_F)} = \frac{2E_F}{3N} \tag{3}$$

Note that Equation (3) is equivalent to Kubo's original result ($\Delta = 4E_F/3N_{atoms}$) which was derived by assuming a monovalent metal and ignoring the spin degeneracy of electron states [2]. Clearly, Δ approaches zero as N grows. Knowing the value of the Fermi energy from the free-electron model for the metal in question as a material parameter [3], Equation (3) yields predictions for the critical size, both in terms of diameter (d_{cr}) and the number of electrons ($N_{cr} = 2\,E_F/3\Delta$), when $\Delta \approx k_B T_R$ and quantum size effects will emerge. Table 1 shows these estimates. It is interesting to note that while the values of N_{cr} vary for more than sixfold, the varying valence electron densities equalize the differences and the d_{cr} values are consistently within 1.6–2 nm for different metals.

In addition to creating a fundamental band gap at the Fermi energy, decreasing the size of metal clusters into nanometer-scale has another fundamental effect for single-electron levels, as will be discussed next.

2. Electron shell structure

Shell structure, i.e. bunching of single-electron levels into groups of (nearly) degenerate energy, is a fundamental property of fermions confined in small systems. It is observed for nucleons in atomic nuclei, electrons in ordinary atoms, in metal nanoclusters and in semiconductor quantum dots, and arises from the symmetry properties of the Schrödinger equation governing the solutions to their quantum states. Historically, the concept of fermionic shell structure and symmetry principle in quantum mechanics were tied together in the Nobel prize of Physics 1963. Half of the prize was given to Eugene Paul Wigner 'for his contribution to the theory of the atomic nucleus and the elementary particles, particularly through the discovery and application of fundamental symmetry principles' and the other half was shared by Maria Goeppert Mayer and J. Hans D. Jensen 'for

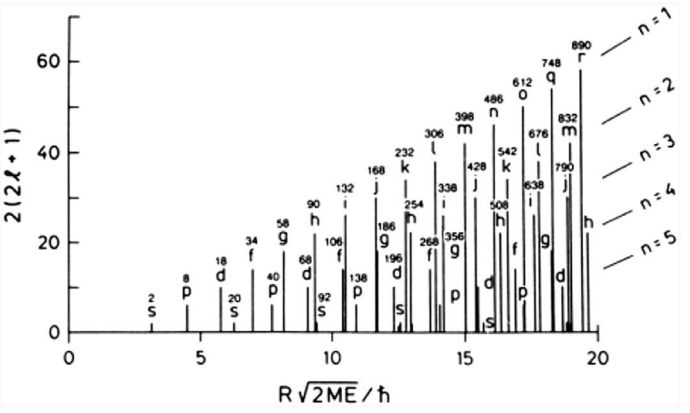

Figure 2. Shell structure of non-interacting fermions in an infinite spherical well. Solutions to the radial Schrödinger equation are grouped into sub-shells according to the radial quantum number (l) with degeneracy of $2(2l + 1)$. The cumulative number of fermions needed to fill all levels up to each sub-shell is shown. The shells are ordered according to an increasing momentum (x-axis). Reproduced by permission from Ref. [4]. Copyright American Chemical Society 1991.

their discoveries concerning nuclear shell structure'.[1] In fact, theories first worked out for nuclear shell structure in 1950's greatly fertilized the field of metal cluster physics in 1980's and 1990's.

The basics of the shell structure can be grasped by considering quantum mechanics of non-interacting fermions in simple forms of radial potentials, solved routinely as an exercise in undergraduate physics courses. Figure 2 shows the degeneracies ($2(2l + 1)$) of solutions to the radial Schrödinger equation for the 3D infinite spherical well with a 'square box shape', organized to the increasing order in energy according to the angular momentum (l) sub-shells [4]. Note that it is customary to label each set of sub-shells by a 'principal' quantum number starting always from $n = 1$ ($1s$, $1p$, $1d$, …; $2s$, $2p$, $2d$, …). This notation differs from electron shells in hydrogen-like atoms where additional rules between quantum numbers arise due to the $1/r$ potential between electrons and the point-like nucleus. Figure 2 clearly shows that angular momentum sub-shells at higher energies start to group together; this is seen already in the set of $2d$–$1h$–$3s$ subshells that accommodate electrons between the major shell-closing ('magic') numbers of 58 and 92. Furthermore, details of the radial potential affect sensitively this grouping. For instance, the infinite harmonic well ($V \propto r^2$) has high degenerate levels at strong magic numbers of 40, 70, 112, 168…, but when the shape of the potential is modified by increasing anharmonicity, finally reaching a shape of the square well, many of the sub-shells split and group together in a new way. This gives rise to the often-quoted series of magic numbers 2, 8, 18, 20, 34, 40, 58, … (Figure 3).

Deformation from 3D radial symmetry modifies the shell structure in a different way [5,6]. Reducing the spherical symmetry to spheroidal, two of the principal axes of the cluster remain the same while the third one is different. This gives

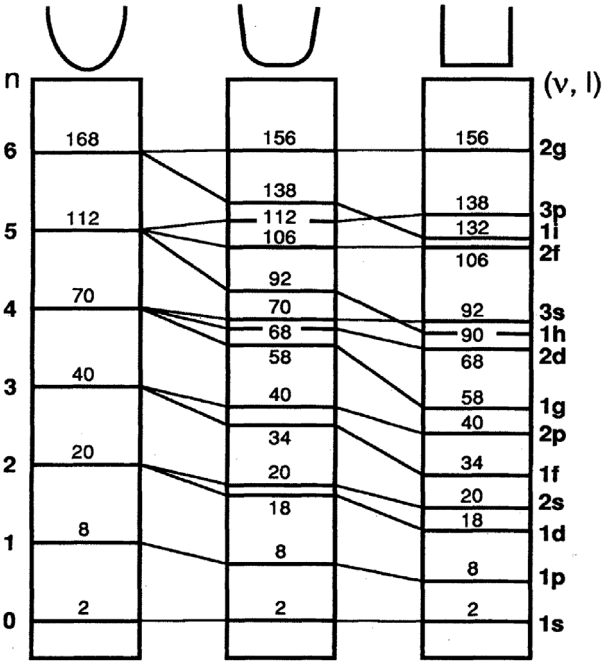

Figure 3. Energy levels of non-interacting fermions in various 3D infinite potential wells (from left: harmonic, intermediate anharmonic, square well). The numbers above levels denote cumulative shell-filling electron counts. Quantum numbers (principal and angular momentum) specifying each shell are given on the right. Reproduced by permission from Ref. [6]. Copyright American Physical Society 1993.

rise to prolate (cigar-like) and oblate (disk-like) shapes. In the field of nuclear physics, Nilsson [7] worked out the effect of spheroidal deformations to nucleon shell structure in 1950's and similar ideas were applied for alkali metal clusters by Clemenger in 1980's [8]. The 'Clemenger–Nilsson' model was successful in explaining the observed relative abundance (based on cluster energetics and stability) of sodium clusters in the early molecular beam experiments in 1980's [9]. Shape deformations are discussed more below in the context of models for interacting electron gas.

3. Interacting electron gas – the jellium model

The Hamiltonian problem for condensed matter systems

$$H\Psi = E\Psi \tag{4}$$

is easy to write up but impossible to solve accurately. The reason lies in ψ which is the hugely complicated many-body wave function of the system, depending on principle on the positions of all the atomic nuclei $\{\mathbf{R}_{i,\, i=1,\, \ldots,\, Na}\}$ and all the electrons $\{\mathbf{r}_{j,\, j=1,\, \ldots,\, Ne}\}$:

$$\Psi = \Psi\left(\mathbf{R}_1, \ldots, \mathbf{R}_{Na}; \mathbf{r}_1, \ldots, \mathbf{r}_{Ne}\right) \tag{5}$$

Even after applying the Born–Oppenheimer approximation (which decouples nuclear and electronic motion and considers the electronic system adiabatically relaxed for each fixed configuration of nuclei) the problem is unsolvable due to the many-body nature of the electron–electron interaction. Since 1960s, the density functional theory (DFT) has facilitated a convenient treatment of this many-body problem, by reducing the number of important degrees of freedom from $3N_e$ to just 3 – defining the density of the electrons $\rho(\mathbf{r})$ in the ground state as the key variable instead of ψ. A classic review of how various theoretical treatments have been applied in the study of metal clusters is provided by Brack [5], here the discussion focuses only on the key points to treat the electron–electron interactions in the electron gas model and what additional insight the electron gas models are able to yield beyond the 'toy models' discussed above.

In DFT, the total energy of the electron–ion system in the electronic ground state is a function of the (valence) electron density $\rho(\mathbf{r})$ of the ground state: (Equation (6))

$$E[\rho] = T_s[\rho] + E_{xc}[\rho] + \int \left\{ V_1(\mathbf{r})\rho(\mathbf{r}) + \frac{1}{2}\rho(\mathbf{r}) \left[e^2 \int \frac{\rho(\mathbf{r}')}{|\mathbf{r} - \mathbf{r}'|} d^3r' \right] \right\} d^3r + E_I \tag{6}$$

where T_s is the kinetic energy of a single-particle (Kohn–Sham, KS) reference system with the same electron density as the true system, E_{xc} is the quantum-mechanical exchange-correlation energy, V_I is the Coulomb energy between ion cores and valence electrons, the fourth term is the Coulomb self-energy of the valence electrons and E_I is the energy of the ion system. The electron density is expressed as a sum over occupied states whose wave functions are represented by the KS virtual orbitals $\varphi(\mathbf{r})$ (Equation (7)):

$$\rho(\mathbf{r}) = \sum_{i=1}^{wN} |\varphi_i(\mathbf{r})|^2 \tag{7}$$

where w is the number of valence electrons per atom in the system of N atoms. In the limit of weak ion core – valence electron interactions (good approximation for instance for alkali metals), the density of the (positive) ion cores is approximated as constant in space over the volume of the cluster, with the normalization that it produces the total positive background charge that neutralizes the total negative charge of the valence electrons (Equation (8))

$$\int \rho(\mathbf{r}) d^3r = wN \tag{8}$$

This approximation is commonly termed as the *jellium* model – perhaps due to the fact that the electron gas is living in a 'jelly-like' medium made out of averaged ion density instead of discrete ions. This model, with several sophistications, was

broadly applied in many of the pioneering theoretical studies in the field of metal cluster physics in 1980's and early 1990s [5,10,11].

Apart from simple non-spherical deformations such as spheroidal shapes, it is also of interest to study electron shell structure in jellium systems where the background density has various polyhedral shapes. This is relevant particularly for ligand-stabilized metal clusters where the metal cores often assume polyhedral shapes due to constraints from the ligand shell. Due to numerically efficient DFT codes, it is now possible to solve the KS equations virtually for any shape of the background jellium density.

Figure 4 shows symmetry analyses of KS states solved self-consistently for five common polyhedra and their comparison to a sphere. The systems were solved for 92 electron states inside the polyhedra, out of which 58 states were occupied providing an electron density corresponding to the density of bulk gold, and the electron–electron interaction was treated by the local density approximation (LDA). The symmetry of the KS wave functions $\varphi_i(\mathbf{r})$ was analyzed by decomposing them into angular momenta by calculating weights $c_{i,l}(R_0)$ (Equation (9))

$$c_{i,l}(R_0) = \sum_m \int_0^{R_0} r^2 dr |\phi_{i,lm}(r)|^2 \tag{9}$$

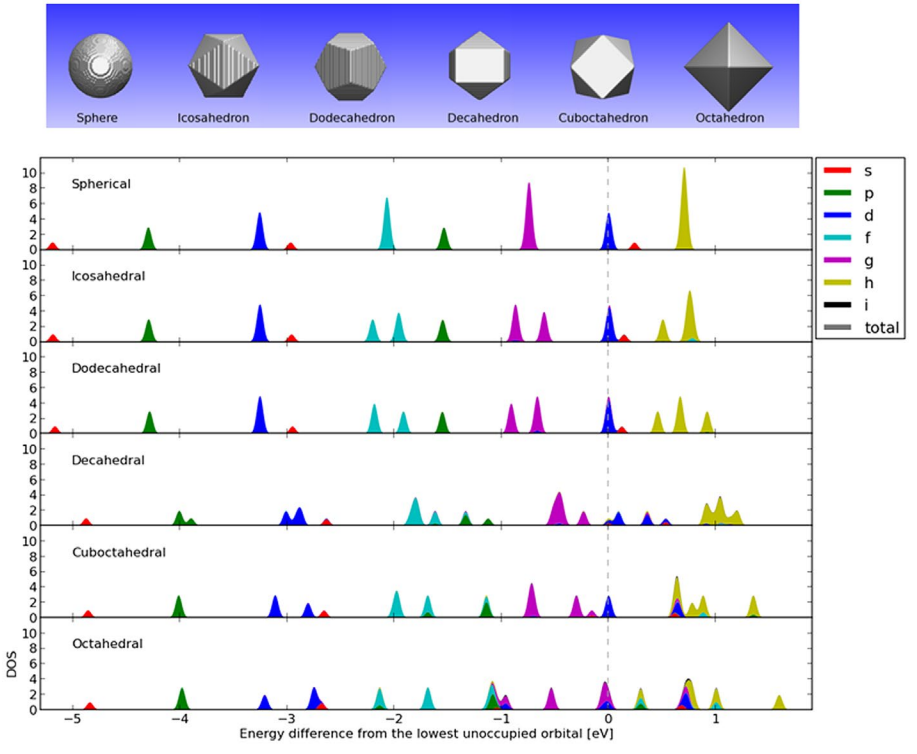

Figure 4. Electron shells obtained in a fixed-background DFT–LDA jellium calculation for various shapes (shown on top) of the background density. The systems contain 58 electrons corresponding to the 6*s*-electron density of bulk gold. The LUMO state ('59th electron') is marked by a dashed vertical line (Kaappa and Häkkinen, unpublished).

where (Equation (10))

$$\phi_{i,lm}(r) = \int d\hat{r} Y^*_{lm}(\hat{r})\varphi_i(\vec{r}) \tag{10}$$

is the projection of a given wave function onto spherical harmonics Y_{lm}. Here, R_0 is a radius of a sphere where the symmetry analysis was done.

58 and 92 are magic shell-closing numbers for the spherical well as shown in Figures 2 and 3. Figure 4 shows that all the considered polyhedral (icosahedron, dodecahedron, decahedron, cuboctahedron and octahedron) preserve the same shell ordering as seen in the spherical system: 1*s*, 1*p*, 1*d*, 2*s*, 1*f*, 2*p* and 1*g* for the occupied states and 2*d*, 3*s* and 1*h* for the unoccupied states. However, the polyhedral shapes split many of the angular momentum shells. 1*p* and 2*p* shells are split in the decahedron, 1*d* and 2*d* are split in decahedron, cuboctahedron and octahedron, and 1*f*, 1*g* and 1*h* shells are split in all polyhedra. Cuboctahedron and octahedron mix some of the states with different angular momenta together.

DFT – jellium calculations and state symmetry analysis can be done also for quasi-2D systems. Figure 5 shows circular, hexagonal and triangular disks with a thickness corresponding to two monolayers of gold containing 60 electrons at the density of bulk gold, with several unoccupied states solved as well. State symmetries can be identified using a similar decomposition into angular momenta as for 3D systems. Figure 6 visualizes the electron orbitals of some of the lowest energy states for the three considered shapes, making it is easy to visually identify most of the low angular momentum states. It is important to realize that the flat systems obey drastically different shell-closing sequence from 3D systems. The

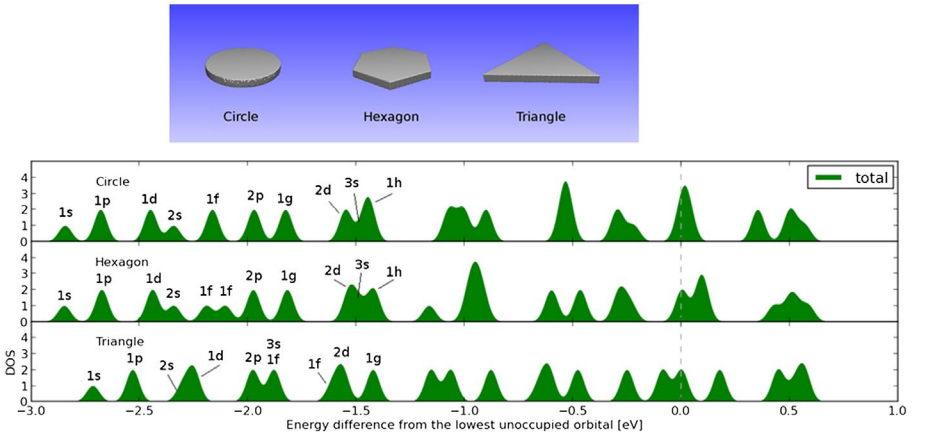

Figure 5. Electron shells obtained in a fixed-background DFT–LDA jellium calculation for flat circular (disk), hexagonal, and triangular shapes of the background density. The systems contain 60 electrons corresponding to the 6*s* electron density of bulk gold and a thickness of two gold monolayers. The LUMO state ('61st electron') is indicated by the dashed vertical line (Kaappa and Häkkinen, unpublished).

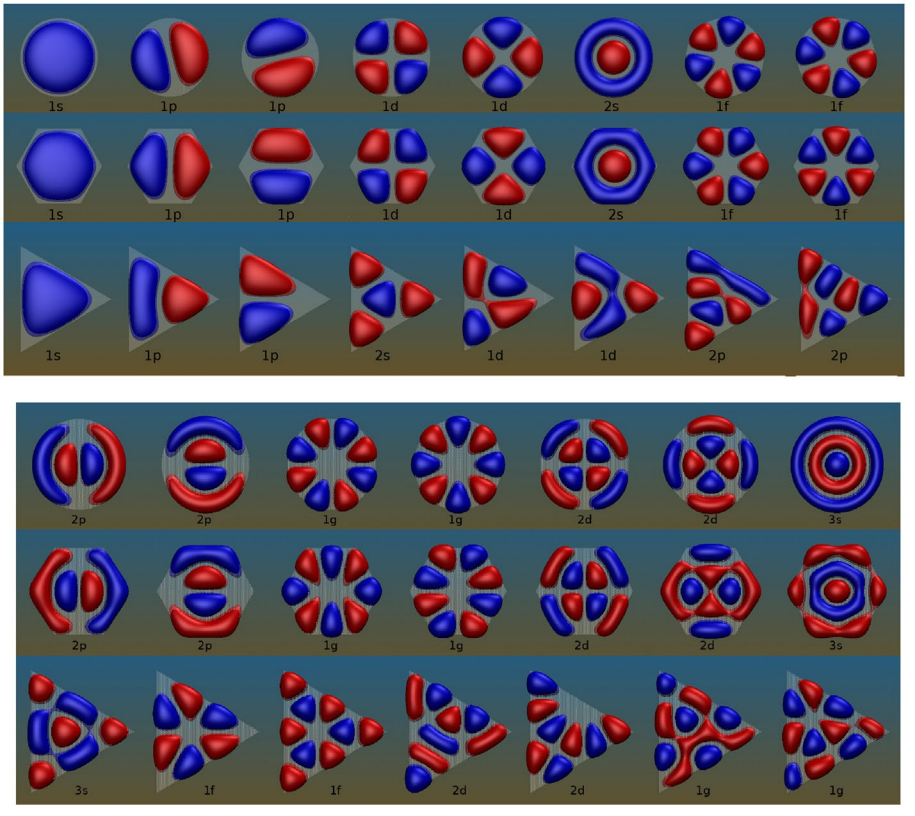

Figure 6. Shapes of the electron orbitals corresponding to the 15 lowest energy states of the flat clusters shown in Figure 5 (Kaappa and Häkkinen, unpublished).

overall degeneracy of the states is either 1 (*s*-states) or 2 (all the higher states), giving a sequence of 'magic numbers', for instance, for a circular disk as 2, 6, 10, 12, 16, 20, 24, … Figure 5 shows that six is quite a strong magic number (meaning that the energy gap to the next shell is large) for all of the considered 2D shapes (circular, triangular and hexagonal). This may in fact be connected to the concept of 'aromaticity' in carbon clusters or carbohydrates: the aromaticity of the benzene molecule C_6H_6 arises from six delocalized C(p) electrons forming a delocalized pi-system in a hexagonal confinement, and the configuration is thus analogous to $1S^2\ 1P^4$. In a similar way, stability of gas-phase Au_6 cluster was attributed back in 2000 to the shell-closing of six Au(6s) electrons in a 2D triangular structure [12]. It can be remarked that a combined experimental and theoretical study in 2003 clearly showed the importance of the six-electron system as a stabilizing factor in gas phase experiments for a series of planar Au_5X^+ clusters [13].

The 2D jellium treatment can straightforwardly be extended to shell (or 'onion shell') structures, by defining volumes (shells) of varying background density or missing background density and solving for the self-consistent electronic structure. In fact, by doing so, one recover yet another series of magic electron

numbers 2, 8, 18, 32, 50, 72, … that correspond to $1S^2\ 1P^6\ 1D^{10}\ 1F^{14}\ 1G^{18}\ 1H^{22}$ … shell fillings, i.e. with ever-larger angular momenta but lacking radial nodes. This series of numbers corresponds to the series of magic numbers for 'spherical aromaticity' [14].

As the examples shown above, considering electron shells in different pre-defined shapes of the positive background density give useful information on the effect of the shape on the splitting of angular momentum sub-shells. However, one can ask an important question: *given the number of electrons, what is the optimal shape of the electron cluster, corresponding to the minimal energy*? A conventional approach to this question involves studies of a large number of different fixed shapes and making conclusions from comparison of their total energies. This approach is completely analogous to a study into optimal structure (lowest-energy isomer) of clusters with real atoms. However, an elegant method development in mid-1990s introduced the 'ultimate' jellium model where the positive background density is allowed to freely deform during the iterative solution of the electronic problem so that in the converged , the system is charge-neutral in each point in space [15]. This brings about a special situation where all the Coulomb energies in the system (electron–electron, electron–ion and ion–ion) cancel exactly and the energetics is defined only by the quantum mechanical kinetic energy of the KS electrons and the exchange-correlation energy:

$$E[\rho] = T_s[\rho] + E_{xc}[\rho] \tag{11}$$

Another special feature of this model is that there are no free parameters, and the bulk limit of the model gives a universal 'jellium material' with the electron density parameter of $r_s = 4.18$ Bohr units (r_s is defined as the radius of a sphere that holds one electron). This density, most closely realized by alkali metals sodium and potassium, minimizes the total energy per electron in an infinite bulk electron gas. A slight drawback of the model is that only neutral systems can be considered due to the requirement of charge cancellation by electrons and the background at each point in space.

Figures 7 and 8 shows the optimal shapes of electron clusters from 2 to 22 electrons, calculated from the ultimate jellium model with LDA and taking spin polarization into account. It is important to realize that the obtained shapes are free from any shape constraints, i.e. all possible multipolar deformations can occur. The evolution of the shape for the smallest clusters from 2 to 8 electrons is easily understood by considering shapes of the single-particle s, p_x, p_y and p_z orbitals. 3- and 4-electron clusters have one and two electrons in one of the p-orbitals – say $p_{x,}$ which makes the electron density axially symmetric and prolate. The initial symmetry degeneration of p orbitals is broken by the Jahn–Teller deformation which favors shape deformation rather than a symmetric shape with paramagnetic spin configuration (such as occupation of spin triplet $1s^2\ 1p_x^{2/3}p_y^{2/3}p_z^{2/3}$ for a spherical 4-electron cluster). The 5th and 6th electrons go to the p_y orbital, making the 6-electron cluster axially symmetric oblate. Note that Figure 5 indicates 6 as

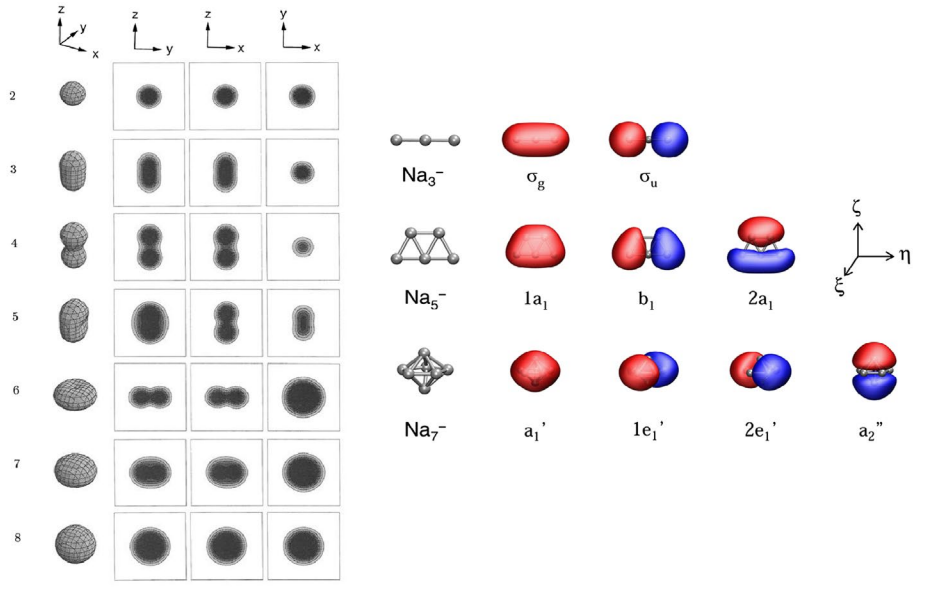

Figure 7. Left: Ground state densities of electron cluster from two to eight electrons, obtained from the 'ultimate' jellium model. The 3D constant density surface is plotted at the value of 38% of the bulk density. Reproduced by permission from Ref. [15]. Right: orbitals for the valence electrons of Na_3^-, Na_5^- and Na_7^- from atomistic DFT calculations. Angular-dependent photoelectron spectroscopy of these clusters can be interpreted using this orbital scheme. Reproduced by permission from Ref. [16]. Copyright 2014 American Chemical Society.

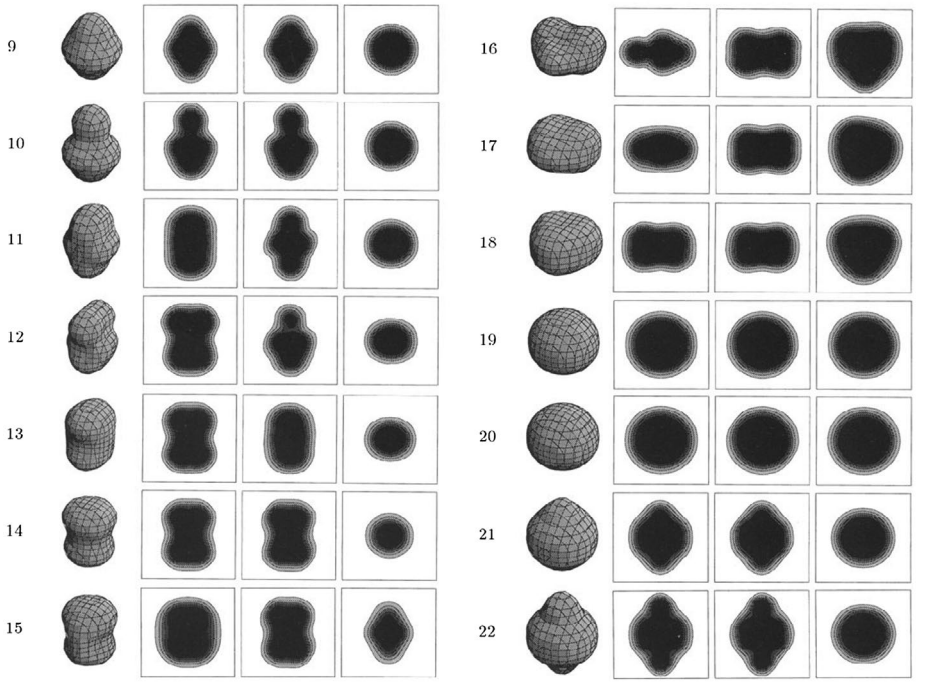

Figure 8. Same as Figure 7, but from 9 to 22 electrons. Reproduced by permission from Ref. [15].

the magic electron number for circular, hexagonal and triangular disks as well – there the orbital filling is identical to this case. Clusters with 7 and 8 electrons fill the remaining p_z orbital which makes the 8-electron cluster a magic, spherical $1s^2\ 1p^6$ octet.

Atomistic DFT calculations for sodium clusters have predicted minimum-energy structures that rather well reflect the shapes of the electron density . As a recent example, photoelectron imaging spectroscopy of sodium cluster anions Na_3^-, Na_5^- and Na_7^- [16]. was interpreted in terms of atomic structures and electron orbitals as shown in Figure 7.

Clusters with 9–20 electrons can be understood in terms of filling 1*d* and 2*s* orbitals (Figure 8). Generally, elongated shapes are observed in the beginning of the *d*-shell filling up to the mid-shell 13- and 14-electron clusters, after which the shapes turn oblate. Some of the clusters however are missing both axial and inversion symmetry. Likewise, 21- and 22-electron clusters can be understood in terms of the 1f shell filling.

Shape isomers exist and were largely discussed in the original paper. [15] For instance, two shapes were obtained with an almost degenerate energy for the 18-electron cluster: a non-spherical shape as shown in Figure 8 and a spherical shape with a reduced density at the center ('hollow-like'). Figure 9 demonstrates that even the 8-electron cluster, assumed usually as the spherical $1s^2\ 1p^6$ octet configuration discussed above, has several isomeric shapes that are energetically quite close to each other. The shapes shown in Figure 9 suggest that these isomeric

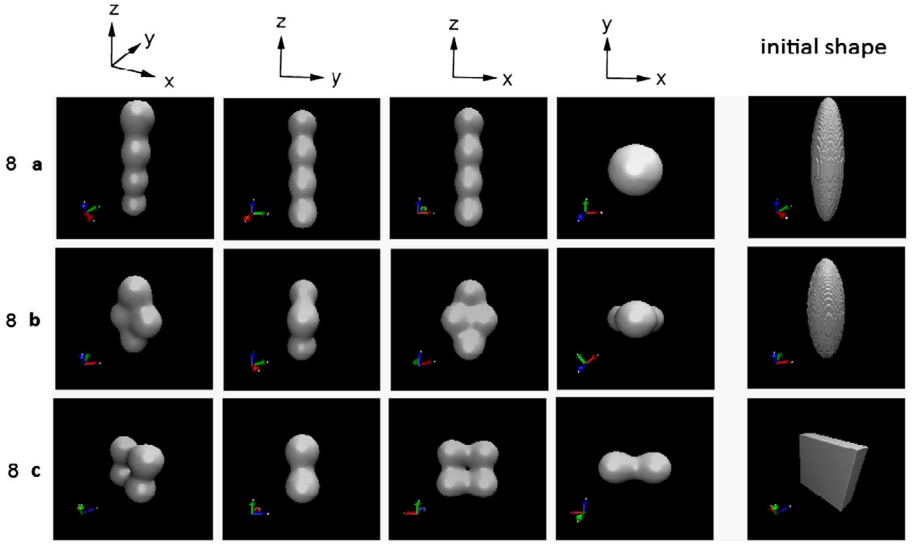

Figure 9. Three shape isomers for the 8-electron cluster in the 'ultimate' jellium model. The converged shapes were started from electron densities shown on the right. The energies per electron are 8a: −1.831 eV; 8b: −1.855 eV; 8c: −1.841 eV; as compared to −1.915 eV for the ground state sphere shown in Figure 7 (Selenius and Häkkinen, unpublished).

clusters could be understood as 'clusters of electron clusters', i.e. consisting of linked, spherical 2-electron systems. It is important to realize that a cluster with a 'magic' number of electrons may not always be spherical.

The ultimate jellum model discussed above deals with the ideal 'jellium material' with r_s = 4.18 Bohr units and may thus miss important electron–electron interaction effects when metal clusters with considerably smaller density (larger r_s) need to be considered. In fact, a recent work by Aguado [17] studied a large number of structural isomers of Cs clusters up to 80 atoms. A remarkable exchange splitting was observed for many of the larger clusters, consistent with highly symmetric atomic structures. This brings an important new concept of a possibility to have 'magnetic superatoms' where the magnetism arises from the exchange interactions between delocalized electrons alone.

The remaining of this paper highlights three classes of systems where electron shell structure has played an important role for interpreting the physical properties of the system. First, a prototypical system of gas phase sodium clusters is briefly discussed. This is perhaps the best-known system that has been instrumental in the development of the field since the classic experiments in 1980s that connected the abundance and several physical properties of small sodium [9] and other alkali [18] clusters to electron shell models [5,6,10,11,19]. Second, flat gold clusters grown on insulating surfaces were predicted [20] to have observable quantum dot states which were later confirmed using scanning tunneling microscopy and spectroscopy techniques [21]. Finally, metal clusters that are synthesized by wet chemistry and stabilized by an organic ligand layer form an intriguing class of novel nano-structured materials. The 'superatom' model [22] that has been motivated by the knowledge from gas phase cluster physics has turned out to be quite successful for rationalizing experimental observation particularly for systems that are close to spherical.

4. Metal clusters in gas phase: sodium as the prototypical case

The electron shell structure of various metal clusters in gas phase has been extensively probed by photoelectron spectroscopy (PES). It is an attractive, 'non-intrusive' method to probe the 'intrinsic' binding energy distribution of valence electrons in mass-selected clusters, without the need to couple the clusters to the environment as would be required in a conventional solid-state conductance experiment, which would both be technically very demanding and change the clusters' intrinsic electronic structure. The method was pioneered in mid-1980s, first in studies of metal-oxide molecules [23] and later applied to a large number of studies of alkali, alkali-earth and noble metal clusters [24–37]. The laser excitation is routinely done with UV–vis lasers which cover a range of several electron volts in valence binding energies particularly for metal cluster anions whose electron affinity is typically of the order of 0.5–2 eV (which by definition is the binding energy of the 'outermost electron' or the 'most weakly bound electron'). Studying

the cluster anions is beneficial also due to the fact that the PES gives information about the electron energy level structure of the clusters in the final neutral state – although, due to the vertical nature of the process, in the atomic configuration corresponding to the anion. In the theoretical side, several schemes based on the KS single electron concept are frequently used for interpreting the experimental binding energy distributions (photoelectron spectra) [29,33,34,38–45]. In fact, due to the lack of direct methods to determine the atomic structure of metal clusters in gas phase, it has become a practice to compare the KS density of states calculated for either single isomers or isomer ensembles (time-averaged over atomistic dynamic simulations) to experimental PES data. This allows for indirect assignment of the plausible structures in several cases. Electron shell effects are clearly seen for smaller clusters in the PES data, as an example of the shell closing for sodium cluster cations at 40 electrons, see Figure 10, but atomic packing for certain 'magic' sizes such as the icosahedral Na_{55}^{+} is strongly suggested by the data

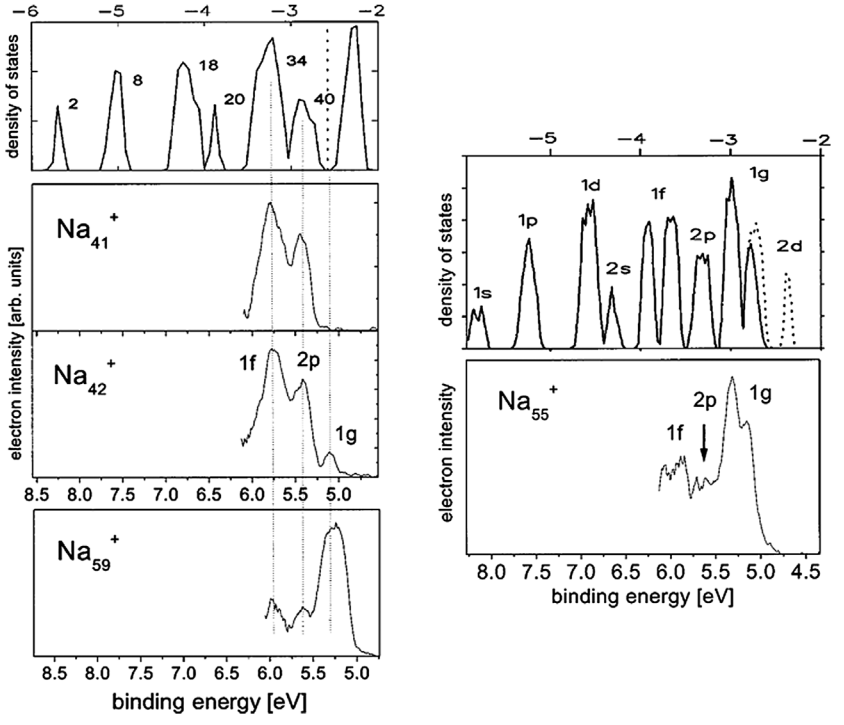

Figure 10. Left: Photoelectron spectra of sodium cluster cations with 41, 42 and 59 atoms (40, 41 and 58 electrons, respectively, three lower panels) compared to DFT simulations of the electron density of states of a neutral, approximately spherical Na_{40} cluster [44] shown in the top panel. The progression of the observed PES peaks matches very well with the predicted electron shell structure around 40 electrons, showing the successive emergence of 1*f*, 2*p* and 1*g* shells. Right: Comparison of the PES data of Na_{55}^{+} to the calculated [42] density of states of the icosahedral Na_{55}^{+}. Based on this comparison, 1*f*, 2*p* and 1*g* shells can be assigned in the PES data. The dashed lined in the top panel denotes the unoccupied part of the density of states. Reproduced by permission from Ref. [26]. Copyright 2002 American Physical Society.

as well (Figure 10). Recent extensive DFT calculations [30,31,45] seem to agree that electron shell effects are mostly dominant up to about 40 electrons, while icosahedral Mackay packing motif is clearly observed for the expected sizes of 55, 147 and 309 atoms, with anti-Mackay face-by-face growth dominating in the intermediate ranges.

Recently, Köster and co-workers [46] suggested an interesting possibility to have a magnetic cluster Na_{55}^{+}, arising from a special connection of highly symmetric (icosahedral) atomic structure and a filling of an electronic sub-shell (G_g point symmetry) with 54 electrons.

5. Two-dimensional shell structure: gold clusters on supported oxides

Recent progress in the controlled growth of ultrathin (a few monolayers, ML, thick) insulating alkali metal-halide or metal-oxide films has made it possible to fabricate well-defined substrates for spectroscopic studies of metal particles and molecule–metal systems [47–54]. While these films are thick enough to isolate an adsorbate electronically from the metal support, they are thin enough to enable tunneling from or to the scanning tunneling microscope (STM) tip under imaging conditions. This facilitates investigations of nanoscale metal–insulator–metal systems, where new insights can be gained into (i) factors defining the electronic structure, (ii) the charge state(s) of the adsorbate and (iii) the molecule–metal bond formation. Several studies have been focusing on gold adatoms and nanoclusters on metal-oxides, motivated by the catalytic activity of such systems.

Walter et al. [20] considered the electronic structure of small gold clusters on magnesia surfaces by doing DFT computations on clusters bound to an oxygen vacancy (color center) on a bulk MgO or to non-defected thin MgO film supported by another metal. One such example is a flat Au_{20} cluster at the color center of magnesia (Figure 11). The atomic structure of the cluster can be described by '19 + 1', i.e. one atom pins the cluster to the defect and 19 atoms form a roughly hexagonal closely packed layer. Many metallic properties of bulk gold can be understood by considering it as a simple monovalent (6*s*) metal, and theory indeed

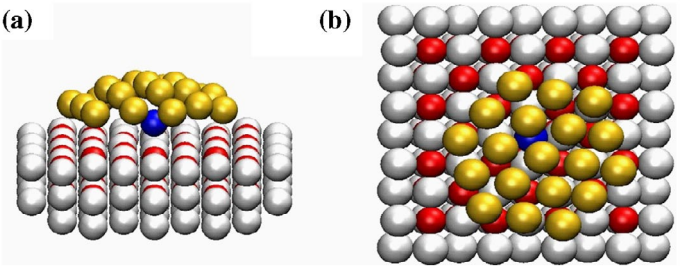

Figure 11. A side view (a) and a top view (b) of a flat, roughly hexagonal model cluster Au_{20} bound at an oxygen vacancy on MgO. The blue sphere is the Au atom closest to the vacancy. Reproduced by permission from Ref. [20]. Copyright 2007 American Physical Society.

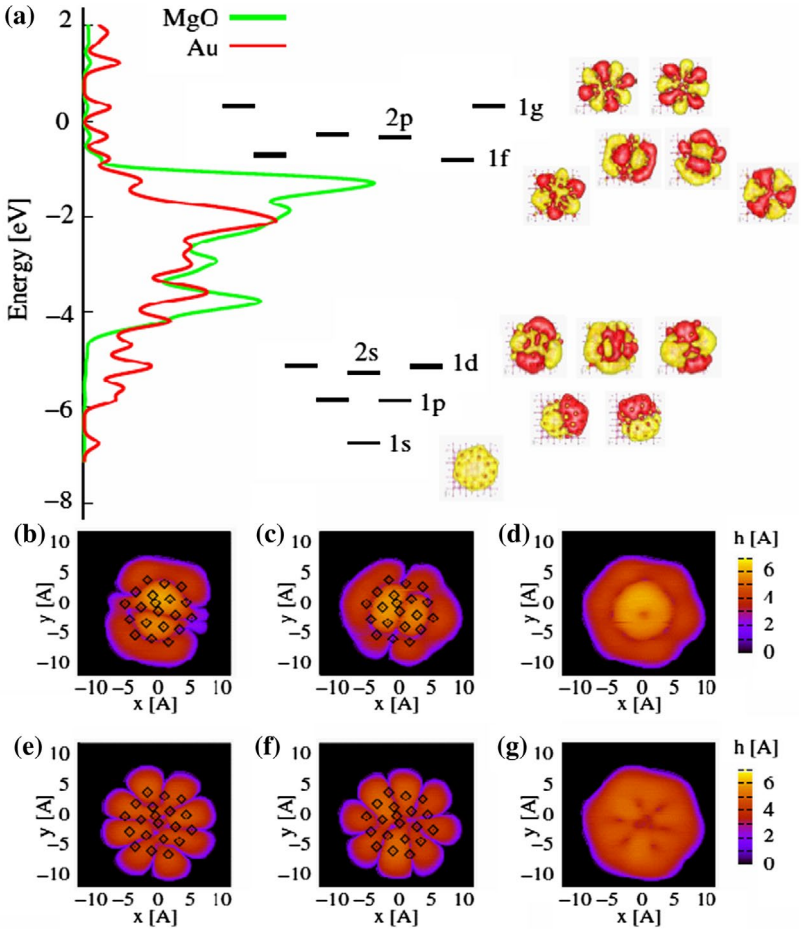

Figure 12. (a) Left: Local density of electron states calculated for the system shown in Figure 11. The energy levels of the KS states with a clear delocalized character are indicated in the middle, and the corresponding wave functions are plotted on the right. The simulated STM pictures (b) and (c) show the two occupied, 2*p*-like states below the Fermi energy. (d) shows the sum of (b) and (c). (e) and (f) show the first two empty states and (g) their sum. The atom positions are indicated by diamonds in (b), (c), (e), and (f). Reproduced by permission from Ref. [20]. Copyright 2007 American Physical Society.

predicts delocalized states in small gas phase gold clusters [55]. The computed electronic structure of the MgO-supported Au_{20} cluster is shown in Figure 12. As is well known, the gold 5*s*–6*s* electrons spread out to a wide mixed band (from the highest occupied level, denoted as zero energy, down to −7 eV in Figure 12). At the bottom of the band, several delocalized states can be recognized whose symmetry and energy ordering resemble a simple physical model of a 2D Fermi gas confined by a harmonic potential (Figure 13). In the middle of the band, the states are predominantly linear combinations of Au(5*d*) orbitals. Around the highest occupied cluster, delocalized 'quantum dot' states are again found. Counting the number and symmetries of the occupied states yields a sequence of $1s^2\ 1p^4\ 2s^2\ 1d^4\ 1f^4\ 2p^4$, with

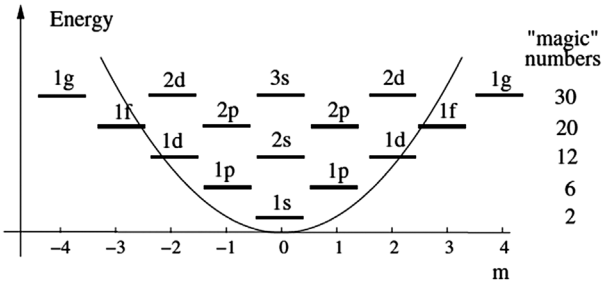

Figure 13. Energy levels and number of electrons for shell closings of the 2D harmonic oscillator model for a planar quantum dot. Reproduced by permission from Ref. [20]. Copyright 2007 American Physical Society.

$1g^4$ as the first unoccupied state. The sequence of the symmetries follows fully the quantum dot model, except that the degeneracies for subshells $1d$–$2s$ and $1f$–$2p$ are broken most likely due to the facts that the atomic symmetry of the cluster deviates from perfect circular symmetry, and the true effective potential in the DFT calculation for gold electrons deviate from the harmonic dot potential. The DFT computations in Ref. [20] also considered flat gold clusters supported on thin MgO films on top of metal supports, and found qualitatively similar conclusions for the existence of shell structures of delocalized Au(6*s*) states.

Since the highest occupied states of the gold clusters lie in the energy gap between the valence and conduction bands of the MgO support (Figure 12), the work of Walter et al. also predicted that the quantum dot states of gold clusters could be detected by means of STM. This was indeed realized by Lin et al. [21] who observed nucleation of small flat gold clusters on an ultrathin MgO/Ag support. A few of the observed clusters could be assigned to precise atomic geometries by comparing results to atomistic DFT simulations on corresponding systems that produced information on the symmetries of cluster states in the MgO band gap. A notable result from this work is that the flat clusters can be rather highly negatively charged, since the support transfers about 0.2 electron charge per cluster atom, meaning that a cluster of about 20 atoms can have an excess charge of −4 units. This can have important consequences to catalytic reactions involving charge transfer to adsorbed molecules [56–59]. Similar charge transfer between the support and gold clusters takes place also on thick, doped oxide films, allowing for control of the dimensionality of electronic properties of oxide-supported gold nanostructures [51,60,61].

6. Ligand-stabilized metal nanoclusters

In recent years, ever-increasing numbers of chemically stabilized (‘passivated’) metal clusters have been synthesized, and successful structural characterizations have opened a fascinating view on how metal atoms organize in the nanometer

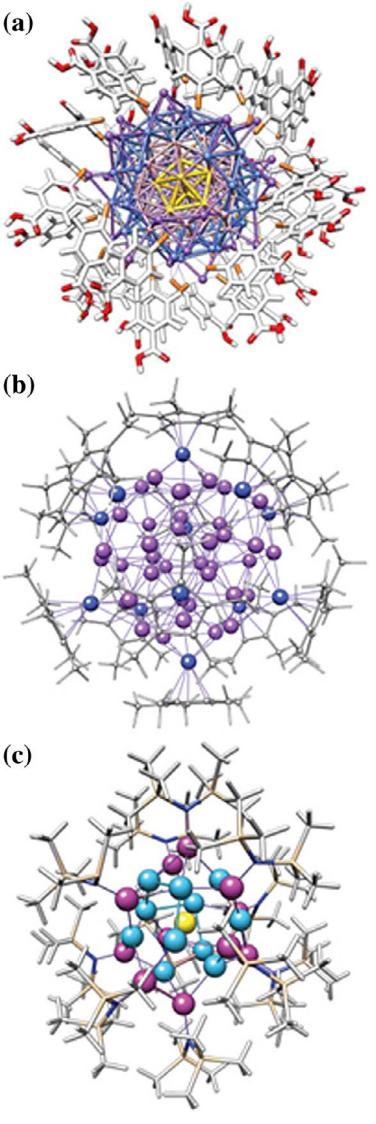

Figure 14. Visualization of ligand-stabilized metal nanoclusters composed of three different metals: (a) Protected gold cluster, $Au_{102}(SC_6H_5COOH)_{44}$ (b) Protected aluminum cluster, $Al_{50}(C_5(CH_3)_5)_{12}$ (c) Protected gallium cluster, $Ga_{23}(N(Si(CH_3)_3)_2)_{11}$. The colored spheres denote metal atoms in various atom shells of the core and the organic layer is shown by sticks. A few ligands have been removed in the front for a better view of the core. Reproduced by permission from Ref. [74]. Copyright 2011 American Physical Society.

scale [22,62–72]. The large database of solved structures has given a treasure trove for theoretical analysis. It has been confirmed numerous times that electron shell structure does play a role and is a useful concept for understanding electronic and optical properties of chemically stabilized metal clusters (the so called monolayer protected clusters or MPCs). This has led to the use of the concept of 'superatom'

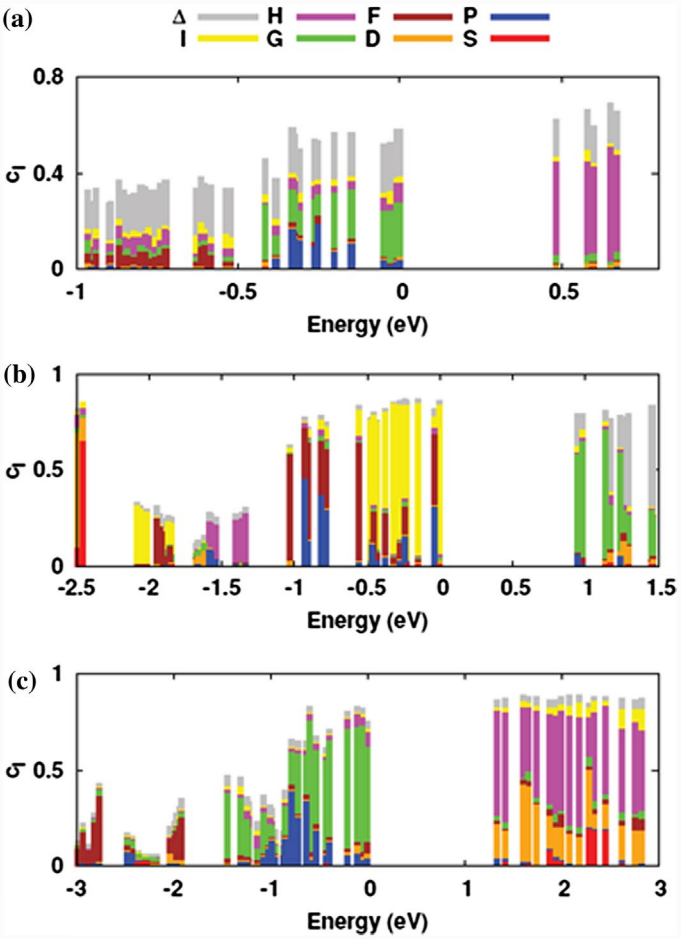

Figure 15. Superatom analysis: angular momentum coefficient c_l from Equation (9) ($l = 0,1, \ldots ,6$) as a function of the energy of the projected KS orbital for the systems shown in Figure 14. The HOMO state is at zero energy. Reproduced by permission from Ref. [74]. Copyright 2011 American Physical Society.

Table 2. The correlation between the electronic structure and binding characteristics of O_2 for partially protected gold clusters 1–5, with binding of dioxygen at Au(111) as reference. Negative binding energy denotes endothermic adsorption. D and D_C are the overall and metal core diameters, respectively, n_e and n_e' are the free electron counts of the fully and partially protected clusters, HL gap is the HOMO–LUMO gap of the fully protected cluster which is activated towards oxygen adsorption by removing part of the ligand layer. BE(O_2) is the binding energy of dioxygen on the activated clusters and d(Au–O) and d(O–O) are the binding distance of dioxygen to gold and O–O bond distance, respectively. From Ref. [78].

		D (nm)	D_C (nm)	n_e	HL gap (eV)	Ligand removed	n_e'	BE(O_2) (eV)	d(Au–O) Å	d(Au–O) Å
1	$Au_{11}(PH_3)_7Cl_3$	1.2	0.9	8	2.03	Cl	9	0.95	2.17	1.31
2	$Au_{25}(SR)_{18}^{-1}$	1.6	0.9	8	1.25	$Au_2(SR)_3$	9	0.72	2.24	1.31
3	$Au_{39}(PH_3)Cl_6^{-1}$	1.8	1.5	34	0.85	Cl	35	0.59	2.25	1.32
4	$Au_{102}(SR)_{44}$	2.2	1.5	58	0.53	$Au(SR)_2$	59	0.08	2.19	1.30
5	$Au_{144}(SR)_{60}$	2.4	1.7	84	0.08	$Au(SR)_2$	85	−0.15	2.22	1.29
6	Au(111) surface							−0.54	2.26	1.24

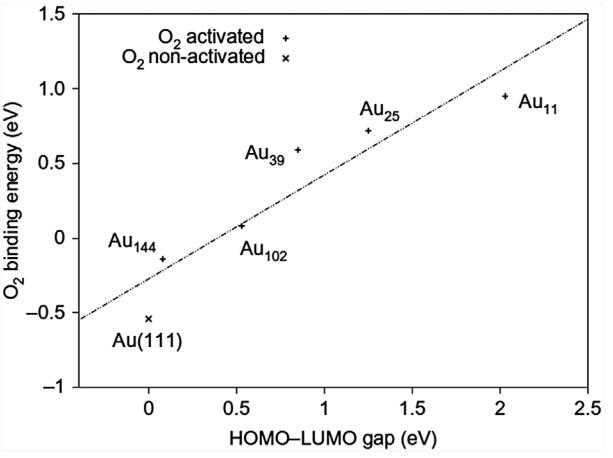

Figure 16. Correlation between the binding energy of O_2 to partially protected clusters 1–5, shown in Table 2, and the HOMO–LUMO gap of the corresponding fully protected cluster. The clusters are labeled by the gold atom count. Although all the clusters activate the O–O bond, only clusters 1–3 (derived from Au_{11}, Au_{25} and Au_{39}) bind O_2 appreciably (by more than 0.5 eV). For comparison, the result for O_2 adsorption on the Au(111) surface is also shown. In that case, the O_2 remains neutral and the O–O bond is not activated. Note that the binding of O_2 to the Au_{144} cluster and Au(111) surface is metastable (endothermic). Reproduced by permission from Ref. [78]. Copyright 2010 Macmillan Publishers Ltd.

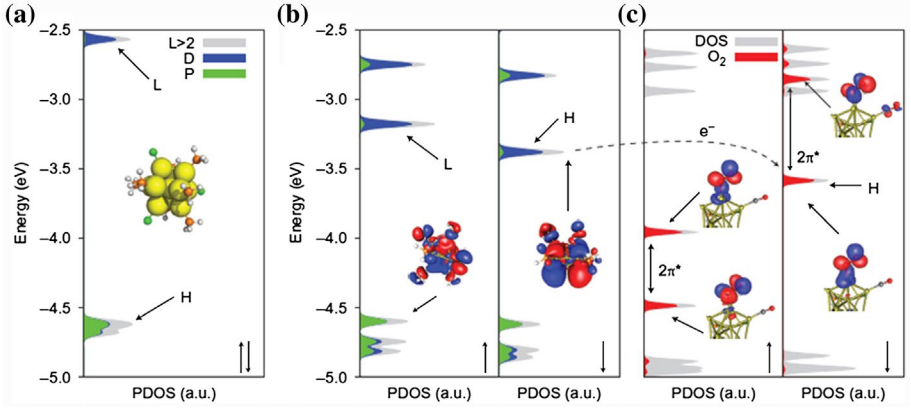

Figure 17. (a) HOMO and LUMO states of the fully protected $Au_{11}(PH_3)_7Cl_3$ cluster. These states are composed of Au(6*s*) states delocalized over the metal core. The green and blue show the major center of mass angular momentum character assigned to the states by projection to spherical harmonics inside the metal, indicating that the HOMO has the superatom *P* symmetry and LUMO has *D* symmetry. (b) Spin-polarized states in the partially protected $Au_{11}(PH_3)_6Cl_2$ cluster. H and L refer to HOMO and LUMO, respectively. The HOMO of the partially protected cluster has *D*-symmetry, as does the LUMO of the fully protected cluster in (a). One electron has thus been transferred to this state over the HOMO–LUMO gap of the fully protected cluster. The *P* and *D* symmetries of the H- and L-orbitals are visualized. (c) On O_2 adsorption, the *D*-symmetric HOMO state in (b) is depleted completely and the electron is transferred to one of the $2\pi^*$ states of O_2, lying in the HOMO–LUMO gap of the gold cluster. This $2\pi^*$ state is empty in the neutral O_2 triplet. Au, yellow; Cl, green; P, orange; H, white; C, grey; O, red. Reproduced by permission from Ref. [78]. Copyright 2010 Macmillan Publishers Ltd.

in the field of MPCs as well, just as it has been used for decades in the field of gas phase metal clusters [73].

Generally, the composition of the ligand-stabilized clusters that have N metal atoms (M), S charge-donating ligands (L), Y charge-withdrawing ligands (X) and an overall charge z can be written as $[L_S M_N X_Y]^z$. In addition, the ligand layer may include ligands that are neither charge donating nor withdrawing. The count of 'free' or delocalized electrons is defined by the simple formula

$$n_e = NV_M - YV_X + SV_L - z \tag{12}$$

where V_M, V_X and V_L are the valence numbers of the metal and the ligands [22]. It is clear that this formula may be generalized to intermetallic clusters as well including all the metal types and their valences.

As an example, the electronic structure of three different systems, consisting of different metals (Au, Al, Ga) and different organic ligand layers, was recently compared by DFT calculations.[73] Figure 14 shows their compositions and atomic structures as determined from single-crystal X-ray diffraction: $Au_{102}(SC_6H_5COOH)_{44}$ (Ref. [75]), $Al_{50}(C_5(CH_3)_5)_{12}$ (Ref. [76]) and $Ga_{23}(N(Si(CH_3)_3)_2)_{11}$ (Ref. [77]). All the ligands in these systems are one-electron withdrawing ligands, so Equation (12) yields the free electron counts of 58 (102 − 44), 138 (3 × 50 − 12) and 58 (3 × 23 − 11) for the gold, aluminium and gallium compounds, respectively. The symmetries of HOMO and LUMO orbitals were analyzed employing Equations (9) and (10), and the results are shown in Figure 15**.** It is seen that for both the 58 electron systems (Au_{102} and Ga_{23}), the symmetry changes from 1G to 1H over the HOMO–LUMO gaps (with a strong mixing of 2D for the gallium cluster) hence for the 138 electron Al_{50} cluster, the symmetry changes from (predominantly) 1I to 2G. These results are in agreement with the shell model in an approximately spherical system.

Equation (12) predicts that the free electron count n_e could be controlled by changing the number of electron-withdrawing or electron-donating ligands. In particular, partially protected clusters could be made electronically 'active' towards electron transfer reaction such as dioxygen binding and reduction, by promoting one or more electrons over the HOMO–LUMO gap of the protected, stable cluster. Several clusters were studied in this respect (Ref. [78] and Table 2). A surprisingly clear correlation between the HOMO–LUMO gap of the (non-activated) cluster and dioxygen binding to the activated cluster was found (Figure 16**)**. In the limit where the HOMO–LUMO gap approaches zero, the binding of dioxygen turns endothermic. Figure 17 illustrates the electron transfer upon dioxygen activation. One phosphine and one chlorine ligand were removed from the fully protected, neutral $Au_{11}(PH_3)Cl_3$ cluster, which renders the partially protected $Au_{11}(PH_3)Cl_3$ to be a 9-electron system where the electron at the HOMO level is actually transferred over the HOMO–LUMO gap of the parent cluster. When O_2 and CO are co-adsorbed on the available gold sites at the partially protected cluster, the HOMO electron transfers to the $2\pi^*$ orbital of O_2 and activates the O–O bond,

making the cluster effectively an 8-electron system again. Mechanisms like this may be important to understand the reactivity of the ligand layer and inter-cluster reactions [79].

7. Conclusions

The concept of the electronic shell structure has been a fundamental one in the field of cluster science for over 30 years. This brief review discussed its origin and validity in three distinct fields comprising fee gas-phase metal clusters, clusters supported on insulating surfaces and clusters stabilized chemically by an organic ligand layer. Experiments on free gas-phase metal clusters have shown that the electronic shell structure is not just of academic interest but creates a real driving force behind systematic behavior of the cluster morphology particularly for Group I alkali metal clusters, that is, tendency to 'spherical' structures for sizes that correspond to magic electron-shell closing numbers. Group II, X, XI and XII elements display similar physics, however they have a larger tendency to directional binding and the *s–d* hybridization masks out some of the features of shell structure. Scanning tunneling microscopy and spectroscopy techniques have been used to probe the electronic states of metal clusters on insulating oxide thin films. Clusters that are close to circular symmetry have been found to exhibit sequence of states close to E_F that resemble fermionic states in a 2D harmonic quantum dot. Finally, metal clusters protected and stabilized by an organic ligand layer constitute a rapidly growing topical field of nanostructured materials. Electron shell structure is discernible particularly in the smallest systems. This has led to a useful concept of 'superatom' that allows rationalization of a vast amount of observations on chemical stability, reactivity and optical properties.

Note

1. http://www.nobelprize.org/nobel_prizes/physics/laureates/1963/

Acknowledgements

I am indebted to all the past and present members of my group as well as to all in-house and external collaborators. The computational resources have been provided by CSC – the Finnish IT Center for Science.

Disclosure statement

No potential conflict of interest was reported by the author.

Funding

This research has been supported by the Academy of Finland.

References

[1] H. Fröhlich, Physica 4 (1937) p.406.
[2] R. Kubo, J. Phys. Soc. Jpn. 17 (1962) p.975.
[3] C. Kittel, *Introduction to Solid State Physics* (7th ed.), Wiley & Sons, Hoboken, NJ, 1996.
[4] T.P. Martin, T. Bergmann, H. Goehlich and T. Lange, J. Phys. Chem. 95 (1991) p.6421.
[5] M. Brack, Rev. Mod. Phys. 65 (1993) p.677.
[6] W.A. de Heer, Rev. Mod. Phys. 65 (1993) p.611.
[7] S.G. Nilsson. Dan. Mat. Fys. Medd. 29 (1955) p.16.
[8] K. Clemenger, Phys. Rev. B 32 (1985) p.1359.
[9] W. Knight, K. Clemenger, W. deHeer, W. Saunders, M. Chou and M. Cohen, Phys. Rev. Lett. 52 (1984) p.2141.
[10] W. Ekardt, Ber. Bunsen Phys. Chem. 88 (1984) p.289.
[11] W. Ekardt, Surf. Sci. 152 (1985) p.180.
[12] H. Häkkinen, Phys. Rev. B 62 (2000) p.R2287.
[13] E. Janssens, H. Tanaka, S. Neukermans, R.E. Silverans and P. Lievens, New J. Phys. 5 (2003) p.46.
[14] M. Bühl and A. Hirsch, Chem. Rev. 101 (2001) p.1153.
[15] M. Koskinen, P.O. Lipas and M. Manninen, Z. Phys. D 35 (1995) p.285.
[16] C. Bartels, C. Hock, R. Kuhnen and B.V. Issendorff, J. Phys. Chem. A 118 (2014) p.8270.
[17] A. Aguado, J. Phys. Chem. 116 (2012) p.6841.
[18] M.M. Kappes, P. Radi, M. Schär and E. Schumacher, Chem. Phys. Lett. 119 (1985) p.11.
[19] W. Ekardt, Z. Phys. B 103 (1997) p.305.
[20] M. Walter, P. Frondelius, K. Honkala and H. Häkkinen, Phys. Rev. Lett. 99 (2007) p.096102.
[21] X. Lin, N. Nilius, H.J. Freund, M. Walter, P. Frondelius, K. Honkala and H. Häkkinen, Phys. Rev. Lett. 102 (2009) p.206801.
[22] M. Walter, J. Akola, O. Lopez-Acevedo, P.D. Jadzinsky, G. Calero, C.J. Ackerson, R.L. Whetten, H. Gronbeck and H. Hakkinen, Proc. Natl. Acad. Sci. USA 105 (2008) p.9157.
[23] J.V. Coe, J.T. Snodgrass, C.B. Freidhoff, K.M. McHugh and K.H. Bowen, J. Chem. Phys. 83 (1985) p.3169.
[24] J. Ho, K.M. Ervin and W.C. Lineberger, J. Chem. Phys. 93 (1990) p.6987.
[25] K.J. Taylor, C.L. Pettiette-Hall, O. Cheshnovsky and R.E. Smalley, J. Chem. Phys. 96 (1992) p.3319.
[26] G. Wrigge, M. Hoffmann and B. Issendorff, Phys. Rev. A 65 (2002) p.063201.
[27] H. Häkkinen, M. Moseler, O. Kostko, N. Morgner, M. Hoffmann and B. von Issendorff, Phys. Rev. Lett. 93 (2004) p.093401.
[28] B.V. Issendorff and O. Cheshnovsky, Annu. Rev. Phys. Chem. 56 (2005) p.549.
[29] M. Moseler, B. Huber, H. Häkkinen, U. Landman, G. Wrigge, M. Hoffmann and B. Issendorff, Phys. Rev. B 68 (2003) p.165413.
[30] O. Kostko, B. Huber, M. Moseler and B. von Issendorff, Phys. Rev. Lett. 98 (2007) p.043401.
[31] B. Huber, M. Moseler, O. Kostko and B. von Issendorff, Phys. Rev. B 80 (2009) p.235425.
[32] A. Aguado, A. Vega, A. Lebon and B. von Issendorff, Angew. Chem. Int. Ed. 54 (2014) p.2111.
[33] J. Akola, M. Manninen, H. Häkkinen, U. Landman, X. Li and L. Wang, Phys. Rev. B 60 (1999) p.R11297.
[34] J. Akola, M. Manninen, H. Häkkinen, U. Landman, X. Li and L. Wang, Phys. Rev. B 62 (2000) p.13216.
[35] H. Häkkinen, B. Yoon, U. Landman, X. Li, H. Zhai and L. Wang, J. Phys. Chem. A 107 (2003) p.6168.

[36] A. Lechtken, D. Schooss, J.R. Stairs, M.N. Blom, F. Furche, N. Morgner, O. Kostko, B. von Issendorff and M.M. Kappes, Angew. Chem. Int. Ed. 46 (2007) p.2944.
[37] N. Shao, W. Huang, Y. Gao, L.-M. Wang, X. Li, L.-S. Wang and X.C. Zeng, J. Am. Chem. Soc. 132 (2010) p.6596.
[38] J.P. Perdew and A. Zunger, Phys. Rev. B 23 (1981) p.5048.
[39] J. Jellinek and P.H. Acioli, J. Chem. Phys. 118 (2003) p.7783.
[40] P.H. Acioli and J. Jellinek, Phys. Rev. Lett. 89 (2002) p.213402.
[41] M. Harris and P. Ballone, Chem. Phys. Lett. 303 (1999) p.420.
[42] J. Akola, A. Rytkönen, H. Häkkinen and M. Manninen, Eur. Phys. J. D 8 (2000) p.93.
[43] M. Walter and H. Häkkinen, New. J. Phys. 10 (2008) p.043018.
[44] A. Rytkönen, H. Häkkinen and M. Manninen, Phys. Rev. Lett. 80 (1998) p.3940.
[45] A. Aguado and O. Kostko, J. Chem. Phys. 134 (2011) p.164304.
[46] J.M. Vásquez-Pérez, G.U. Gamboa, D. Mejía-Rodríguez, A. Alvarez-Ibarra, G. Geudtner, P. Calaminici and A.M. Köster, J. Phys. Chem. Lett. 6 (2015) p.4646.
[47] S. Schintke and W.D. Schneider, J. Phys. Condens. Matt. 16 (2004) p.R49.
[48] J. Repp, G. Meyer, F.E. Olsson and M. Persson, Science 305 (2004) p.493.
[49] J. Repp, G. Meyer, S. Paavilainen, F.E. Olsson and M. Persson, Science 312 (2006) p.1196.
[50] T. Risse, S. Shaikhutdinov, N. Nilius, M. Sterrer and H.-J. Freund, Acc. Chem. Res. 41 (2008) p.949.
[51] G. Pacchioni and H. Freund, Chem. Rev. 113 (2013) p.4035.
[52] K. Honkala, Surf. Sci. Rep. 69 (2014) p.366.
[53] M. Sterrer, M. Yulikov, E. Fischbach, M. Heyde, H.-P. Rust, G. Pacchioni, T. Risse and H.-J. Freund, Angew. Chem. Int. Ed. 45 (2006) p.2630.
[54] B. Yoon, H. Häkkinen, U. Landman, A. Worz, J. Antonietti, S. Abbet, K. Judai and U. Heiz, Science 307 (2005) p.403.
[55] B. Yoon, P. Koskinen, B. Huber, O. Kostko, B. von Issendorff, H. Häkkinen, M. Moseler and U. Landman, ChemPhysChem 8 (2007) p.157.
[56] P. Frondelius, A. Hellman, K. Honkala, H. Häkkinen and H. Grönbeck, Phys. Rev. B 78 (2008) p.085426.
[57] P. Frondelius, H. Häkkinen and K. Honkala, Angew. Chem. Int. Ed. 49 (2010) p.7913.
[58] X. Lin, N. Nilius, M. Sterrer, P. Koskinen, H. Häkkinen and H.-J. Freund, Phys. Rev. B 81 (2010) p.153406.
[59] J. Nevalaita, H. Häkkinen and K. Honkala, Surf. Sci. 640 (2015) p.10.
[60] J. Andersin, J. Nevalaita, K. Honkala and H. Häkkinen, Angew. Chem. Int. Ed. 52 (2012) p.1424.
[61] J. Nevalaita, H. Häkkinen and K. Honkala, Catal. Sci. Technol. (2016). doi:http://dx.doi.org/10.1039/C5CY01839K
[62] T. Tsukuda and H. Häkkinen, *Protected Metal Clusters: From Fundamentals to Applications*, Elsevier, Amsterdam, 2015.
[63] R. Sardar, A.M. Funston, P. Mulvaney and R.W. Murray, Langmuir 25 (2009) p.13840.
[64] R. Jin, Nanoscale 2 (2010) p.343.
[65] T. Tsukuda, Bull. Chem. Soc. Jpn. 85 (2012) p.151.
[66] Y. Negishi, Bull. Chem. Soc. Jpn. 87 (2014) p.375.
[67] C. Aikens, J. Phys. Chem. Lett. 2 (2011) p.99.
[68] H. Häkkinen, Nat. Chem. 4 (2012) p.443.
[69] H. Häkkinen, Chem. Soc. Rev. 37 (2008) p.1847.
[70] A. Fernando, K.L.D.M. Weerawardene, N.V. Karimova and C.M. Aikens, Chem. Rev. 115 (2015) p.6112.
[71] D.E. Bergeron, P.J. Roach, A.W. Castleman, N.O. Jones and S.N. Khanna, Science 307 (2005) p.231.

[72] J. Ulises-Reveles, P.A. Clayborne, A.C. Reber, S.N. Khanna, K. Pradhan, P. Sen and M.R. Pederson, Nat. Chem. 1 (2009) p.310.
[73] P. Jena, J. Phys. Chem. Lett. 4 (2013) p.1432.
[74] O. Lopez-Acevedo, P.A. Clayborne and H. Häkkinen, Phys. Rev. B 84 (2011) p.035434.
[75] P.D. Jadzinsky, G. Calero, C.J. Ackerson, D.A. Bushnell and R.D. Kornberg, Science 318 (2007) p.430.
[76] J. Vollet, J.R. Hartig and H. Schnöckel, Angew. Chem. Int. Ed. 43 (2004) p.3186.
[77] J. Hartig, A. Stößer, P. Hauser and H. Schnöckel, Angew. Chem. Int. Ed. 46 (2007) p.1658.
[78] O. Lopez-Acevedo, K.A. Kacprzak, J. Akola and H. Häkkinen, Nat. Chem. 2 (2010) p.329.
[79] K.R. Krishnadas, A. Ghosh, A. Baksi, I. Chakraborty, G. Natarajan and T. Pradeep, J. Am. Chem. Soc. 138 (2016) p.140.